Cell Reports, Volume *20*

Supplemental Information

Mpp6 Incorporation in the Nuclear Exosome Contributes to RNA Channeling through the Mtr4 Helicase

Sebastian Falk, Fabien Bonneau, Judith Ebert, Alexander Kögel, and Elena Conti

Figure S1

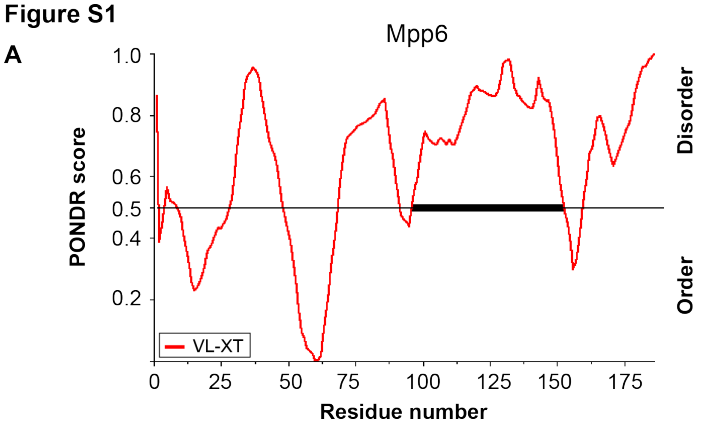

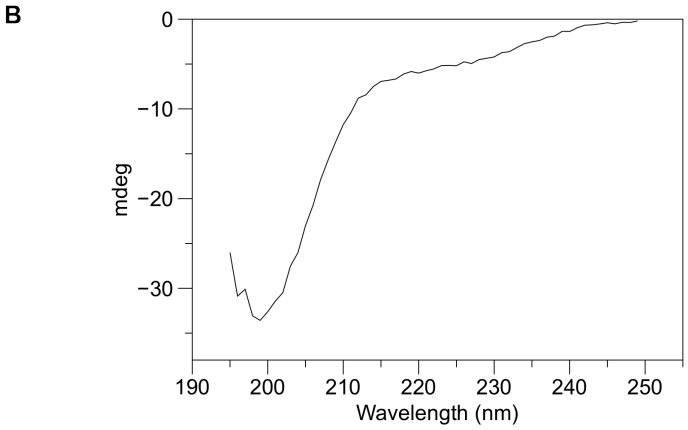

C

```
ScMpp6/1-186      1 MSANNGVTGKLSSRVMNMKFMKFGKTDDEESSNSNTPSNINSDVEPIEQKGKLFGLDDSAWDLNSYKDDLKKIS 74
SpMpp6/1-188      1 ----------MSSKLLSMKFMQRARGIDPKQAEEELSKNIVTDEH---------------WSLAGKVDFLPQKM 49
DrMpp6/1-168      1 M-ANDGGA-KLSKNLLRMKFMQRGLDAEVKKQLDEEEKRIISDEH---------------WFL-----DLPELK 52
HsMpp6/1-160      1 M-AAERKT-RLSKNLLRMKFMQRGLDSETKKQLEEEEKKIISEEH---------------WYL-----DLPELK 52
GgMpp6/1-164      1 M-AGEVKT-KLSKNLLRMKFMQRGLDSQTKKQLDEEEKKIISDEH---------------WYL-----DLPDLK 52

ScMpp6/1-186     75 GKEKKKVKRVVYKKRPNLIISNVGYSELRKPEGVISGRKTFGDNSDDSGSRKRKFDEGEQNED----------137
SpMpp6/1-188     50 TRN------VEYESGYGGLIEENDLESHSNEPNLVQGRASFGLFNKELGEENVDEKDVSKNEEVDVNG----TK113
DrMpp6/1-168     53 AKE------------NHIIEERSFVPC---EDLVYGRMSFKGFNPDVEKLMLLMNAPREEEDEEEEDESMNKM110
HsMpp6/1-160     53 EKE------------SFIIEEQSFLLC---EDLLYGRMSFRGFNPEVEKLMLQMNAKHKAEEVEDE-----TV105
GgMpp6/1-164     53 EKE------------SYIIEERSFIPC---EDLLYGRMSFKGFNPEIEKLMVQINSKSKKEEIEEDD----KM106

ScMpp6/1-186    138 -------EKRDAKDKEFTGSQDDG----------EDEYDLDKLFKDSIKKKKTNHNGKNKNRNSKK------186
SpMpp6/1-188    114 ITDTSELTERERRKQELVSKKAEASRKMEVKAPAKESKKRKVNELSQDVISLHSPKESNARKTKKNKNKKKKR187
DrMpp6/1-168    111 ETDITD-EEMAKRYQSLVES----------------MRKKFAKKRDRSAVSNKEDVNCNVTDDIRPKRAFMKPQ167
HsMpp6/1-160    106 ELDVSD-EEMARRYETLVGT----------------IGKKFARKRDH---ANYEEDENGDITPIKAKKMFLKPQ159
GgMpp6/1-164    107 EADVSD-EEMARRYETLVGT----------------IGKKFLKKRDQRVLHDEDEEENSNTKPKKARKMFLKPQ163
```

Figure S1, related to Figure 1. Mpp6 in an intrinsically disordered and conserved protein. (**A**) Sequence analysis predicts yeast Mpp6 as intrinsically disordered. Bioinformatic disorder prediction analysis of *S. cerevisiae* Mpp6 (1-186) with the program PONDR (Li et al., 1999). (**B**) Analysis of Mpp6 secondary structure using far-UV CD spectroscopy indicates that Mpp6 is unfolded in solution. The far-UV CD spectrum exhibits a pronounced minimum around 200 nm and only weak ellipticity above 210 nm, which is characteristic for unfolded proteins. (**C**) Sequence alignment of full-length Mpp6 with orthologues from the representative species *Saccharomyces cerevisiae* (Sc), *Schizosaccharomyces pombe* (Sp), *Homo sapiens* (Hs), *Danio rerio* (Dr) and *Gallus gallus* (Gg).The level of conservation is indicated by color: from dark blue (high conservation) to white (no conservation).

Figure S2

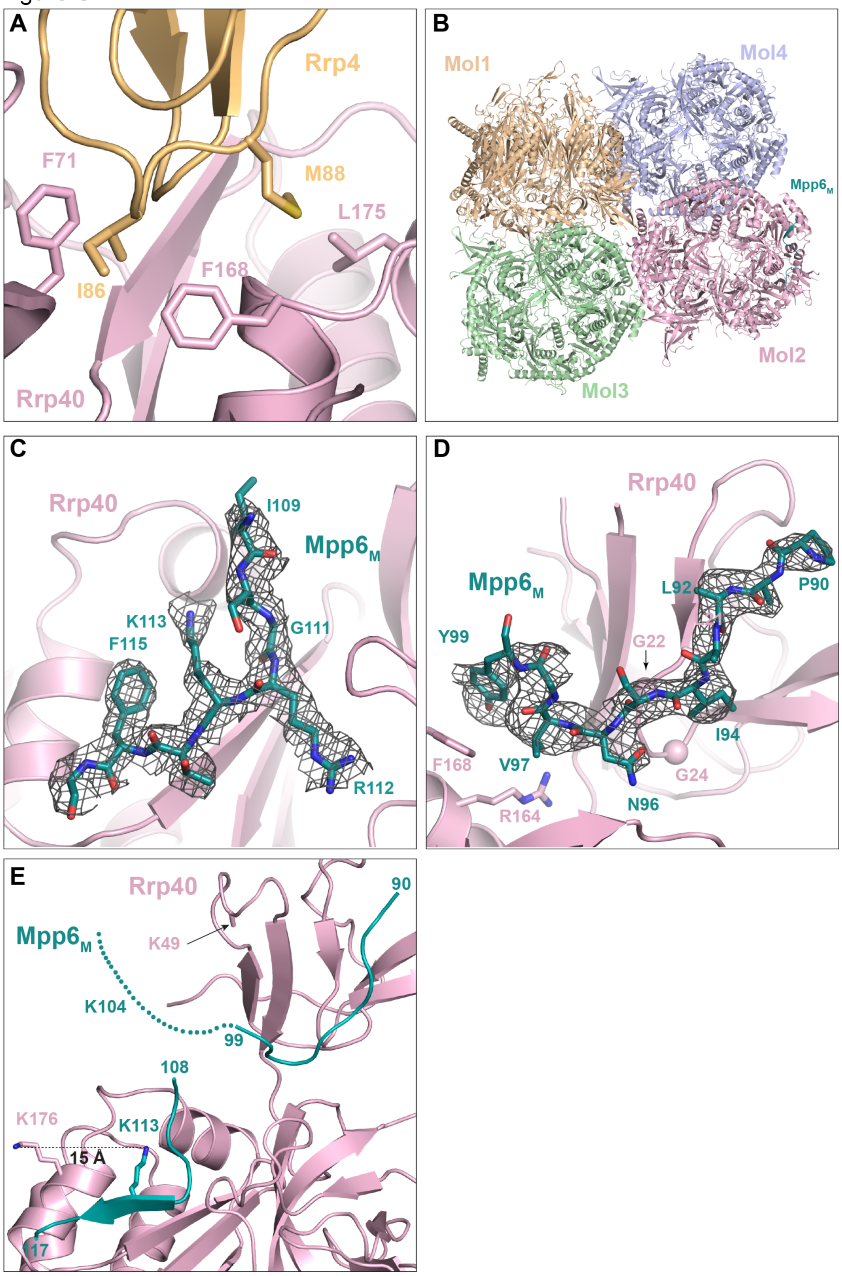

Figure S2, related to Figure 2. Crystallographic analysis of the Exo-9$_{Rrp4mut}$ – Mpp6$_M$ complex. **(A)** Typical Rrp40–Rrp4 interface forming lattice contacts in a representative yeast exosome crystal structure (PDB: 4IFD). Rrp4 is shown in orange and Rrp40 in salmon. Isoleucine 66 and methionine 68 of Rrp4 were mutated to glutamate (Rrp4$_{mut}$) to change crystal packing. **(B)** Packing of the four copies of the complexes present is in the asymmetric unit of the Exo-9$_{Rrp4mut}$ – Mpp6$_M$ crystal. The different copies are colored in brown, salmon, green and blue and related by non-crystallographic symmetry We note that the hydrophobic patch at Rrp4 I66 and Met68 is used to bind the Rrp6 nuclease domain (Makino et al., 2015; Wasmuth et al., 2014; Zinder et al., 2016). When crystallizing exosome complexes in the absence of Rrp6, this hydrophobic patch has a strong tendency to mediate protein-protein interactions with other complexes in the crystal lattice. (**C**) and (**D**) Snapshots of the refined electron density from the Mpp6–Rrp40 interface at the long segment (**C**) and the short segment, fitted tentatively with the Mpp6 sequence from Pro90 to Tyr99 (**D**). The refined 2mFo-DFc map (sharpened with -45 Å^2 B-factor) is contoured at 1.0 σ and superposed with the final model. Rrp40 is colored salmon, Mpp6 in cyan. (**E**) Superposition of Mpp6$_M$ onto the structure of yeast Exo-11 (PDB: 4IFD) to highlight the proximity of the two intermolecular crosslinks between Mpp6 and Rrp40 peptides observed by (Shi et al., 2015).

Figure S3

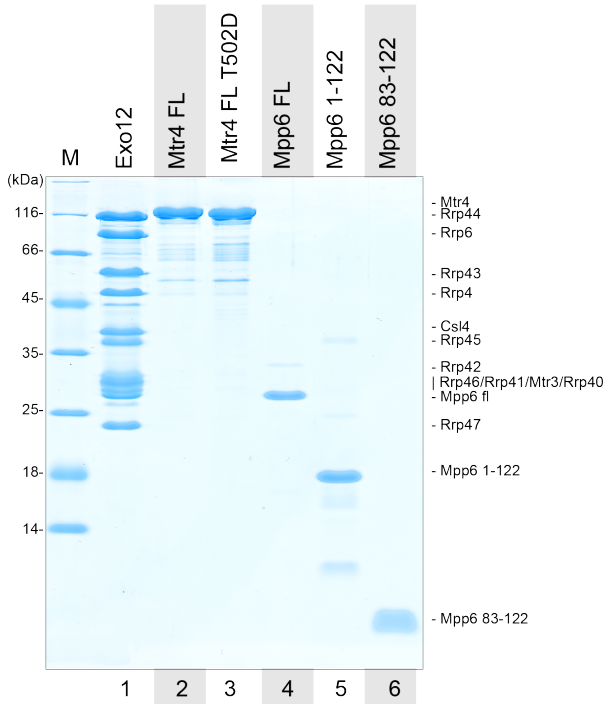

Figure S3, related to Figure 3. Proteins used in RNase protection assay.
15% SDS-PAGE gel stained with Instant Blue (Expedeon) showing the proteins used in the RNase protection experiment. 10 pmol of sample were loaded in lanes 1-4 and 40 pmol of sample in lanes 5 and 6.

Supplemental Experimental Procedures

Recombinant protein expression and purification

S. cerevisiae Mpp6 proteins (full-length, truncations and mutants) were expressed as His-GST-fusions in *E. coli* and purified as previously described (Schuch et al., 2014). The His_6-GST tag was cleaved using 3C protease, when required. Purification and assembly of the yeast exosome was performed as described in (Makino et al., 2013) with the exception that Rrp46 was truncated at the C-terminus (1-223) and Rrp4 at the N-terminus (51-359) to remove regions that were poorly ordered in the previous structures (Kowalinski et al., 2016). *S. cerevisiae* Mtr4 proteins (full-length and truncations) were purified as described in (Falk et al., 2014). The yeast Exo-9 – Mpp6 complex was reconstituted by mixing Exo-9 with 1.2 fold molar excess of Mpp6 full-length followed by gel filtration in a buffer containing 20 mM Hepes/NaOH pH 7.5, 100 mM NaCl and 2 mM DTT.
Purification and assembly of the *H. sapiens* Exo-9 complex was performed as described in (Greimann and Lima, 2008; Kowalinski et al., 2016). Human MPP6 residues 40-83 were tagged at the N-terminus with a His_6-thioredoxin-tag (His-Trx) and at the C-terminus with a $(Ser\text{-}Gly)_3$-linker and eGFP-StrepII-tag (eGFP-StrepII) to reduce proteolytic degradation. The resulting His-Trx-hMPP6-eGFP-StrepII fusion protein was expressed in *E. coli* and purified using Ni- and Streptactin affinity chromatography. The mutants were purified with the same protocols as the wild-type proteins with the exception of the yeast Mpp6-Cys184 substitution, where we replaced 2 mM DTT with 0.5 mM TCEP in the final buffer.

Endogenous protein purification

All yeast strains generated here are derivatives of the base strain BY4741 (MATa his3Δ1 leu2Δ0 met15Δ0 ura3Δ0). General yeast manipulations were conducted by standard methods with transformation by the lithium acetate method (Gietz and Schiestl, 2007). A C-terminal tandem affinity purification tag inspired by (Passmore et al., 2003) was engineered consisting of a 10-residues Glycine-Serine linker preceding a TwinStrep tag, followed by a 3C protease cleavage site and two IgG-binding domains of *Staphylococcus aureus* protein A. Yeast carrying tagged versions of exosome subunits were cultivated in 1 to 2 liters of YPD to an OD_{600} of 1 and harvested by centrifugation. The cell paste was

immediately frozen and pulverised in a freezer/mill (Spex). The powder was resuspended in lysis buffer (250 mM potassium phosphate pH 8.0, 1 mM EDTA, 0.1% NP40 (v/v), 0.5 mM DTT) containing complete protease inhibitor cocktail (Roche), clarified by centrifugation at 18000 g for 15 min and incubated 2 h at 4˚C with IgG-sepharose resin (GE Healthcare). Beads were washed three times with IPP250 (10 mM Tris pH 8.0, 250 mM NaCl, 0.1% NP40 (v/v)), resuspended in cleavage buffer (10 mM Hepes/NaOH pH 7.9, 50 mM KCl, 2 mM $MgCl_2$, 0.1% NP40 (v/v), 0.5 mM DTT) and incubated 2 h at room temperature with 1 µg 3C protease and 750 U Serratia marcescens nuclease. The eluate was incubated with StrepTactin resin (IBA) for 1 h at 4˚C, beads were washed three times with IPP250 and the final complex eluted in IPP250 supplemented with 2.5 mM D-desthiobiotin (Sigma). Eluates were precipitated with Trichloroacetic acid before separation on a 12% SDS PAGE and staining with InstantBlue (Expedeon).

Pull-down assays

For the pull-down reactions of the yeast proteins in Figures 1D and 2C, 1.0 µM of bait protein (GST-Mpp6) was pre-incubated with 1.2 µM of prey (Exo-9) in a in buffer containing 20 mM Hepes/NaOH pH 7.5, 100 mM NaCl, 2 mM DTT and 0.01% (v/v) NP-40 for 1 h at 0°C. Then the sample was incubated with GSH Sepharose (GE Healthcare) for 2 h at 4°C, washed three times with the same buffer, and eluted in 20 mM Tris/HCl pH7.5, 100 mM NaCl, 2 mM DTT, 0.01% (v/v) NP-40 and 30 mM reduced gluthathione. Input and pull-down fractions were analyzed on denaturing 12.5% SDS-PAGE and visualized with Coomassie staining.

For the pull-down reactions of the human proteins in Figures 2D and 2E, a total of 5 µg of tagged bait (His-Trx-$hMPP6^{40-83}$-eGFP-StrepII) was incubated with 1.2 molar excess of untagged prey (human EXO-9) in a volume of 50 µl in pull-down buffer (20 mM Tris/HCl pH 7.5, 100 mM NaCl, 0.01% (v/v) NP-40, 5 mM DTT). The high ionic strength buffer contained 500 mM NaCl instead of 100 mM NaCl. After incubation with GFP-binder resin for 1 h and three washing steps with pull-down buffer the resin was dried and taken up in SDS sample buffer and boiled for 3 min at 95°C to elute bound proteins. Input and pull-down fractions were analyzed on denaturing 12% SDS-PAGE.

RNase protection assay

For the RNase protection assays in Figure 3, the internally labeled 57-mer RNA substrate (5′ - $C(*UC)_{28}$ - 3′) was generated by *in vitro*-transcription in presence of a-^{32}P UTP using the MEGAshortscript kit (Ambion) and purified by poly-acrylamide gel electrophoresis. Typically, 10 pmol protein was mixed with 5 pmol internally labeled RNA in a final reaction volume of 20 µl (final buffer: 50 mM MES pH 6.0, 50 mM NaCl, 5 mM magnesium diacetate, 10% glycerol (v/v), 0.1% NP40 (v/v) and 1 mM DTT). Samples were incubated at 4°C for 1 h before treatment with 0.5 µl RNase A/T1 mix (Thermo Scientific) for 20 min at 20°C. The reaction was stopped by 10x dilution in a buffer containing 100 mM Tris pH 7.5, 150 mM NaCl, 300 mM sodium acetate, 10 mM EDTA and 1% (w/v) SDS. Protected RNA fragments were then extracted twice with phenol:chloroform:isoamyl-alcohol (25:24:1, (v/v/v), Invitrogen), precipitated with ethanol, separated on a 12% (w/v) denaturing poly-acrylamide gel and visualized by phosphorimaging.

Microscale Thermophoresis

For the microscale thermophoresis experiments in Figure 1A, Mpp6 S184C was labeled with red-maleimide following the manufactures protocol (MO-L004 Monolith, NanoTemper Technologies). 50 nM of labeled Mpp6-S184C (Mpp6-S184C*) was incubated with increasing concentrations of unlabeled Exo-9 in 50 mM Tris/HCl pH 7.4, 150 mM NaCl, 10 mM $MgCl_2$, 0.05% (v/v) Tween 20. The Exo-9 concentration series was produced by serial dilution (1:1). Thermophoresis was measured with an LED power of 40% and standard parameters on a NanoTemper Monolith NT.115 machine. Titrations were performed in triplicates and the data were analysed using the Thermophoresis and T-Jump strategy option with the MO software (NanoTemper Technologies).

Circular dichroism

Circular dichroism spectra (Figure S1B) were recorded on a Jasco J-715 spectropolarimeter in a 0.1-cm path length cuvette at 20°C. $Mpp6^{FL}$ was exchanged into a buffer containing 10 mM potassium phosphate pH 7.5, 50 mM sodium fluoride. Eight scans were taken from 250 to 190 nm in 1-nm increments and the scans were averaged, and the buffer spectrum was subtracted.

Crystallization and structure determination

The best diffracting crystals of the Exo-$9_{Rrp4mut}$ – $Mpp6_M$ complex were obtained at 12 mg/ml in 0.1 M Tris/Mops pH 7.5, 30 mM $MgCl_2$, 30 mM $CaCl_2$ and 30% PEG 8000/Ethylene glycol. Crystals were frozen directly from the drops and X-ray data were collected at 100 K at the beamline PXII (X10SA) of the Swiss Light Source (SLS) (Villigen, Switzerland). The crystals belong to the monoclinic space group $P2_1$ with four complexes in the asymmetric unit and diffracted to 3.2 Å resolution. Data processing was performed using the DIALS (Waterman et al., 2016), Xia2 (Winter, 2009) and AIMLESS (Evans and Murshudov, 2013) programs that are part of CCP4i2 (Winn et al., 2011). The structure of the Exo-$9_{Rrp4mut}$ – $Mpp6_M$ complex was solved by molecular replacement using the structure Exo-9 core from (PDB 5JEA) (Kowalinski et al., 2016) using PHASER (McCoy et al., 2007) within Phenix (Adams et al., 2010). Model building was performed using COOT (Emsley et al., 2010) and the structure was refined using phenix.refine (Afonine et al., 2012), Refmac (Murshudov et al., 2011) and Buster (version 2.10.3) (Smart et al., 2012). The stereochemistry of the model was assessed using MolProbity (Davis et al., 2007).

Supplemental References

Adams, P.D., Afonine, P.V., Bunkoczi, G., Chen, V.B., Davis, I.W., Echols, N., Headd, J.J., Hung, L.-W., Kapral, G.J., Grosse-Kunstleve, R.W., McCoy, A.J., Moriarty, N.W., Oeffner, R., Read, R.J., Richardson, D.C., Richardson, J.S., Terwilliger, T.C., Zwart, P.H., 2010. PHENIX: a comprehensive Python-based system for macromolecular structure solution. Acta Crystallogr D Biol Crystallogr 66, 213–221.

Afonine, P.V., Grosse-Kunstleve, R.W., Echols, N., Headd, J.J., Moriarty, N.W., Mustyakimov, M., Terwilliger, T.C., Urzhumtsev, A., Zwart, P.H., Adams, P.D., 2012. Towards automated crystallographic structure refinement with phenix.refine. Acta Crystallogr D Biol Crystallogr 68, 352–367.

Davis, I.W., Leaver-Fay, A., Chen, V.B., Block, J.N., Kapral, G.J., Wang, X., Murray, L.W., Arendall, W.B., Snoeyink, J., Richardson, J.S., Richardson, D.C., 2007. MolProbity: all-atom contacts and structure validation for proteins and nucleic acids. Nucleic Acids Research 35, W375–83. doi:10.1093/nar/gkm216

Emsley, P., Lohkamp, B., Scott, W.G., Cowtan, K., 2010. Features and development of Coot. Acta Crystallogr D Biol Crystallogr 66, 486–501.

Evans, P.R., Murshudov, G.N., 2013. How good are my data and what is the resolution? Acta Crystallogr D Biol Crystallogr 69, 1204–1214.

Falk, S., Weir, J.R., Hentschel, J., Reichelt, P., Bonneau, F., Conti, E., 2014. The Molecular Architecture of the TRAMP Complex Reveals the Organizationand Interplay of Its Two Catalytic Activities. Molecular Cell 55, 856–867.

Gietz, R.D., Schiestl, R.H., 2007. High-efficiency yeast transformation using the LiAc/SS carrier DNA/PEG method. Nat Protoc 2, 31–34.

Greimann, J., Lima, C., 2008. Reconstitution of RNA exosomes from human and Saccharomyces cerevisiae cloning, expression, purification, and activity assays. Meth. Enzymol. 448, 185–210.

Kowalinski, E., Kögel, A., Ebert, J., Reichelt, P., Stegmann, E., Habermann, B., Conti, E., 2016. Structure of a Cytoplasmic 11-Subunit RNA Exosome Complex. Molecular Cell 63, 125–134.

Li, X., Romero, P., Rani, M., Dunker, A., Obradovic, Z., 1999. Predicting Protein Disorder for N-, C-, and Internal Regions. Genome Inform Ser Workshop Genome Inform 10, 30–40.

Makino, D.L., Baumgärtner, M., Conti, E., 2013. Crystal structure of an RNA-bound 11-subunit eukaryotic exosome complex. Nature 495, 70–75.

Makino, D.L., Schuch, B., Stegmann, E., Baumgärtner, M., Basquin, C., Conti, E., 2015. RNA degradation paths in a 12-subunit nuclear exosome complex. Nature 524, 54–58.

McCoy, A.J., Grosse-Kunstleve, R.W., Adams, P.D., Winn, M.D., Storoni, L.C., Read, R.J., 2007. Phaser crystallographic software. J. Appl. Cryst (2007). 40, 658-674 1–17.

Murshudov, G.N., Skubák, P., Lebedev, A.A., Pannu, N.S., Steiner, R.A., Nicholls, R.A., Winn, M.D., Long, F., Vagin, A.A., 2011. REFMAC5 for the refinement of macromolecular crystal structures. Acta Crystallogr D Biol Crystallogr 67, 355–367.

Passmore, L.A., McCormack, E.A., Au, S.W.N., Paul, A., Willison, K.R., Harper, J.W., Barford, D., 2003. Doc1 mediates the activity of the anaphase-promoting complex by contributing to substrate recognition. EMBO J. 22, 786–796.

Schuch, B., Feigenbutz, M., Makino, D.L., Falk, S., Basquin, C., Mitchell, P., Conti, E., 2014. The exosome-binding factors Rrp6 and Rrp47 form a composite surface for recruiting the Mtr4 helicase. EMBO J. 33, 2829–2846.

Shi, Y., Pellarin, R., Fridy, P.C., Fernandez-Martinez, J., Thompson, M.K., Li, Y., Wang, Q.J., Sali, A., Rout, M.P., Chait, B.T., 2015. A strategy for dissecting the architectures of native macromolecular assemblies. Nat. Methods 12, 1135–1138.

Smart, O.S., Womack, T.O., Flensburg, C., Keller, P., Paciorek, W., Sharff, A., Vonrhein, C., Bricogne, G., 2012. Exploiting structure similarity in refinement: automated NCS and target-structure restraints in BUSTER. Acta Crystallogr D Biol Crystallogr 68, 368–380.

Wasmuth, E.V., Januszyk, K., Lima, C.D., 2014. Structure of an Rrp6-RNA exosome complex bound to poly(A) RNA. Nature 511, 435–439.

Waterman, D.G., Winter, G., Gildea, R.J., Parkhurst, J.M., Brewster, A.S., Sauter, N.K., Evans, G., 2016. Diffraction-geometry refinement in the DIALS framework. Acta Crystallogr D Struct Biol 72, 558–575.

Winn, M.D., Ballard, C.C., Cowtan, K.D., Dodson, E.J., Emsley, P., Evans, P.R., Keegan, R.M., Krissinel, E.B., Leslie, A.G.W., McCoy, A., McNicholas, S.J., Murshudov, G.N., Pannu, N.S., Potterton, E.A., Powell, H.R., Read, R.J., Vagin, A., Wilson, K.S., 2011. Overview of the CCP4 suite and current developments. Acta Crystallogr D Biol Crystallogr 67, 235–242.

Winter, G., 2009. xia2: an expert system for macromolecular crystallography data reduction. J. Appl. Cryst (2010). 43, 186-190 1–5.

Zinder, J.C., Wasmuth, E.V., Lima, C.D., 2016. Nuclear RNA Exosome at 3.1 Å Reveals Substrate Specificities, RNA Paths, and Allosteric Inhibition of Rrp44/Dis3. Molecular Cell 64, 734–745.